1. Introduction

Autologous fresh nerves are commonly used in clinical applications for treating peripheral nerve defects. However, an alternative to the autologous nerves is needed because these nerves are available only in limited quantities, and also because their use causes concurrent healthy nerve dysfunction [1, 2]. In general, tissue-derived nerves are always preferable, since they possess a natural internal structure of extracellular matrix components, which can lead to cellular migration and nerve fiber elongation [3–7].

Cadaveric donor grafts are an attractive alternative to autologous nerves, and their supply is potentially unlimited. In 2001, clinical trials for cold-preserved nerve allografts were reported to cause severe peripheral nerve defects [8]. In that report, 6 patients exhibited successful nerve reconstruction by cadaveric nerve allograft transplantation. However, long-term systematic administration of immunosuppressant was required, and even with that degree of treatment, one of the patients still experienced immune rejection. Moreover, it has been reported that the rate of nerve regeneration using cold preserved allogeneic nerves is lower than that using autologous fresh nerves with immunosuppressant treatment [9].

For treatment without an immunosuppressant, various strategies to eliminate the immunogenicity of allogeneic nerves have been explored in different animal models, but the grafts revealed very poor completeness in comparison to that of the autografts [10–12]. The main strategies for reducing the immunogenecity of allografts or xenografts are thermal and chemical pretreatments of nerves [8, 13, 14]. These pretreatments can destroy or remove the donor cells, but the natural internal structure of the nerve tissue remains unchanged.

The thermal process involves repeated cycles of freezing and thawing of donor nerves. This process destroys the allogeneic antigen and eliminates allogeneic cells, and has been reported to decrease the host antigeneic response in some studies [8, 15]. However, the axonal growth in these grafts is slower than it is in fresh autografts or isogeneic grafts, because of the residual allogeneic cells in the graft [13]. The cellular debris in the graft leads to macrophage invasion and basal laminae damage, which delay the nerve regeneration [16–19].

Chemical processes to remove the donor cells with detergents have been studied not only for peripheral nerve tissue [14, 20, 21] but also for cardiac muscle [22], heart valves [23] and pericardium [24]. This process is more effective in removing the donor cells. However, it also causes more damage to the extracellular matrices than thermal pretreatment does [7, 25, 26]. In addition, it is difficult to completely remove the detergent from the graft, and the residual chemicals suppress tissue regeneration. Starting in 2002, decellularized human nerves which are processed with a combination of detergent decellularization, chondroitinase degradation and gamma-irradiation sterilization have been marketed by AxoGen in the USA. The decellularized nerve grafts are superior to the commercially available conduits but not as effective as isografts [27].

We have established a novel decellularization method using a cold isostatic pressuring (CIP) treatment [28]. This method has succeeded in removing the cellular components from pig blood vessels, heart valves and trachea. We have also reported on the excellent reconstruction of endothelial cells, fibroblasts and smooth muscle cells in acellular vessels 12 weeks after the transplantation [28]. Thus, novel allogeneic acellular nerve grafts that possess natural extracellular matrices were prepared by the CIP method and examined in this study. In fact, many studies have been performed to develop novel treatments as an alternative to autografts, and most of the acellular tissue transplantations have been studied using isogeneic transplantation models [2, 20, 29, 30]. However, only a few studies have focused on allogeneic transplantation [8, 21, 26, 31]. Moreover, the regeneration of nerves by pretreated nerve transplantation should be assessed functionally in addition to histological assessment. For example, there have been only a few studies focused on the conduction velocity [20, 32] or myogenic potential [20, 31] of the acellular nerve transplantation. Therefore, for this study, allogeneic acellular nerves were prepared from Lewis rat sciatic nerves, and transplanted into a sciatic nerve gap in SD rats. As a preliminary study, a 10-mm gap of sciatic nerve which is repaired by any other nerve graft substitute, was bridged with our acellular nerve grafts to evaluate their potential in nerve regeneration, and the axonal growth in the allogeneic acellular nerves was evaluated histologically and electrophysiologically.

2. Materials and Methods

2.1. Preparation of Acellular Nerves

All animal studies were performed in accordance with the guidelines of the Ministry of Health, Labour and Welfare of Japan, as well as the guidelines of our institution, and approved by the Institutional Animal Care and Use Committee at the National Cardiovascular Center Research Institute.

Approximately 30-mm lengths of the sciatic nerves were harvested from a male Lewis rat weighing 300–350 g (Japan SLC) and, after trimming their peripheral fat and connective tissues, the nerves were packed in a polyethylene pouch with Ca^{2+}-, Mg^{2+}-free phosphate-buffered saline (PBS; Invitrogen) and the air was expelled. The nerves were then treated with ultra high pressure of 980 MPa at 30°C for 10 min using a Dr. Chef high pressure food processor (Kobe Steel) to disrupt all cells, microorganisms and viruses inside the tissues. The cell debris was washed away by immersing the cells in endothelial cell growth medium (EGM-2 Bulletkit; Lonza) for 2 weeks at 37°C. Then, ethanol/PBS (80:20, v/v) was used to remove phospholipids, which lead to calcification of implants, and was removed by rinsing with PBS for 3 days.

The acellular nerves were morphologically and histologically compared with the untreated nerves. The decellularization efficiency and extra-cellular component morphology were evaluated by hematoxylin and eosin staining (HE staining). Briefly, the samples were fixed with 10% neutralized formalin, then dehydrated and

embedded in paraffin, sectioned at 8–10 μm, and captured on slide glasses. The slide glasses were immersed into Mayer's hematoxylin solution (Wako), rinsed with tap water, and counterstained with eosin solution (Wako).

2.2. Subcutaneous Implantation

The host body reaction to the allogeneic fresh nerves and allogeneic acellular nerves was investigated by subcutaneous implantation into rats. As the allogeneic transplantation model, we used Lewis rats and SD rats as donor and recipient animals, as described by Hudson *et al.* [17]. Three 13-week-old male SD rats (Japan SLC) were anesthetized with isoflurane inhalation. Two incisions were made in the dorsal skin on the back of each of three SD rats, and fresh or acellular nerves of a Lewis rat (10 mm long) were inserted into both subcutaneous spaces. Thus, one fresh nerve sample and one acellular nerve sample was implanted into the back of each of the three rats. After 4 weeks of implantation, all rats were killed humanely and the grafts were resected with the surrounding skin.

Angiogenesis and macrophage infiltration against the grafts was evaluated by HE staining ($n = 3$) and immunostaining for von Willebrand Factor (vWF) ($n = 1$) and CD68 ($n = 3$). All resected tissues with graft were fixed with 10% formalin, dehydrated with gradient alcohol and embedded in paraffin. All nerves were sectioned at 4 μm thickness and the middle parts of the grafts were used for staining. For the primary antibody, anti-vWF antibody (Dako) and anti-CD68 antibody (AbD Serotec) were used, and horseradish peroxidase-conjugated secondary antibody (Dako), 3,3-diaminobenzidine substrate (Dako) and eosin solution (Wako) were used to visualize the cells.

The total numbers of infiltrated cells and macrophages in implants and the number of blood vessels with a luminal structure were calculated. The total numbers of cells and macrophages were analyzed using free imaging soft, ImageJ (NIH). Pictures were taken at 40× magnification, and the numbers of nuclei and stained cells were counted using particle analysis tools included in the software package. In HE staining and immunostaining for CD68, three areas were randomly selected within implanted nerves. Blood vessels with a circular form with vWF positive cells inside the grafts were counted visually.

2.3. Implantation of Graft in the Sciatic Nerve Defect

The allogeneic acellular nerves prepared by CIP treatment were transplanted to rat sciatic nerve defect models. The recipient animals, 6 SD rats, were anesthetized by isoflurane, and both sides of the sciatic nerves were exposed. A 10-mm length of the right-side sciatic nerve was excised, and an acellular nerve graft of the same length was sutured at both stumps of the recipient nerve using 10-0 vicryl (Ethicon) under a microscope. Another side sciatic nerve was excised, and the excised nerve was reversed and sutured in the same way as the autograft control. Four of the transplanted animals underwent electrophysiological and histological study, and the others were only used for histological evaluation.

2.4. Assessment of the Transplanted Nerves

The transplanted grafts were electrophysiologically evaluated by electromyograms in the short-term (158 days; $n = 1$) and long-term (247, 248 and 258 days; $n = 1$ each) experiments. Under anesthesia, both sides of the sciatic nerves were exposed from the proximal to the distal parts of the graft positions. The proximal part of the nerve was hooked with two platinum wire electrodes and stimulated with 1 V monophagic rectangular voltage with 10 μs duration at a frequency of 1 Hz (Nihon Koden). The myogenic potential of the tibial muscle group was recorded by inserting two needle-type electrodes, amplified (Nihon Koden) and acquired by a PowerLab system (AD Instruments). In all cases, 50 traces were recorded and averaged.

In the histological evaluation, sciatic nerves including the graft were resected at 110 days ($n = 1$) and 158 days ($n = 1$) post-operation. The nerves were fixed with 10% neutralized formalin, dehydrated and embedded in paraffin. Then, the tissues were sliced longitudinally in sections of 4 μm thickness each, and the middle parts of the grafts were stained using HE or anti-glial fibrillary acidic protein (GFAP) antibody (Dako), which stains Schwann cells in peripheral nerves. The anti-GFAP was visualized with labeled polymer (Dako) according to the manufacturer's specifications. Hematoxylin staining (Wako) was carried out as a counterstaining measure to visualize the nuclei.

2.5. Statistical Analysis

The total number of cells and macrophages in the subcutaneous implantation experiments was counted. The mean values of all parameters were determined along with their standard deviations. Student's t-tests were applied to determine the statistical significance of differences between numbers of total cells and macrophages in allogeneic fresh or allogeneic acellular grafts. Values of $P < 0.05$ were considered to indicate statistical significance.

3. Results

3.1. Decellularization of Rat Sciatic Nerves

Acellular rat sciatic nerves were prepared by destroying cells using CIP treatment and a washing process. At two time points, i.e., immediately after CIP treatment or after CIP treatment plus 3 weeks of washing, nerves were histologically compared with untreated fresh nerves by hematoxylin and eosin (HE) staining and immunostaining for GFAP (Figs 1 and 2). The results showed that CIP treatment alone could not remove the cells (Fig. 1B). After the washing process, all cells were removed from the tissue, and fiber-like extracellular matrices (ECM) were left behind (Fig. 1C). On the other hand, there were many nuclei present among the dense matrices in the untreated fresh nerves (Fig. 1A). Immunostaining showed that the Schwann cells in the nerves completely disappeared after decellularization (Fig. 2B). These histological observations showed that the decellularization process

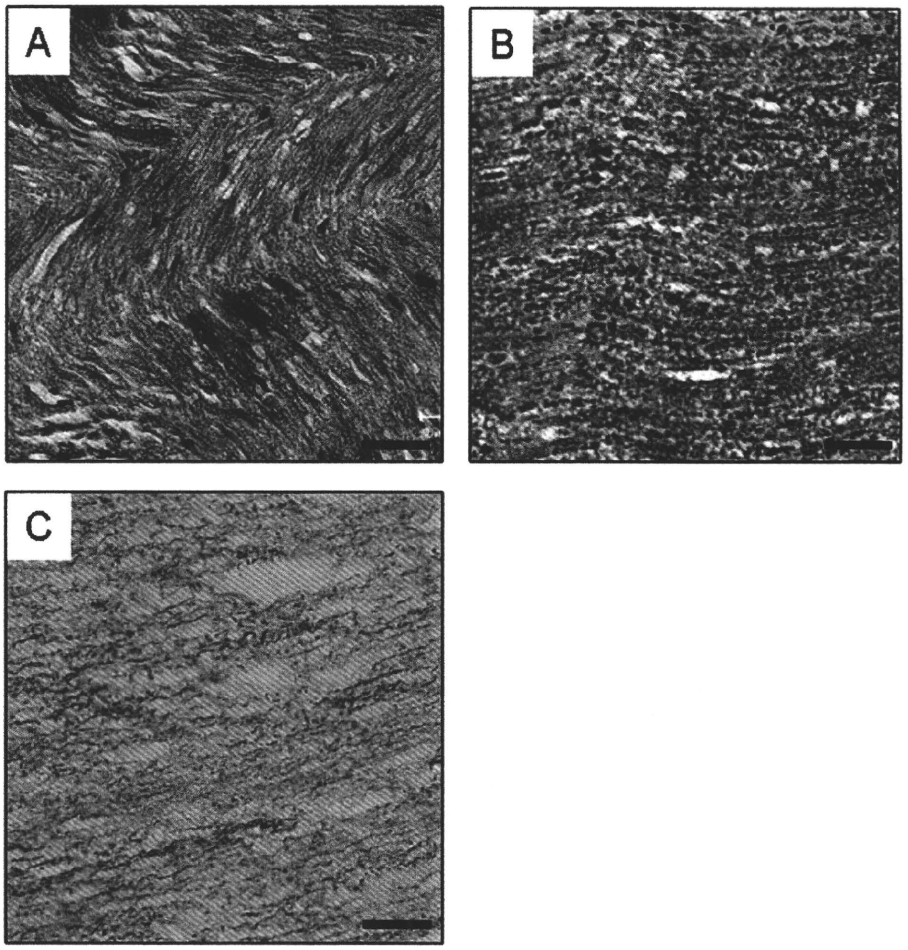

Figure 1. HE staining of a fresh nerve (A), a nerve just after CIP treatment (B) and a nerve after the complete washing process (C). Scale bars = 50 μm.

succeeded in the removal of cellular components while retaining the nerve ECM. The remaining ECM maintained an intrinsic orientation that is expected to be effective for axonal growth.

3.2. Host Body Reactions to Allogeneic Fresh and Acellular Nerves

To investigate how the decellularization process affects the host body reaction, fresh and acellular nerves of Lewis rats were implanted subcutaneously into the SD rats and assessed histologically. At 1 month post-operation, many cells had infiltrated in both grafts (Fig. 3). However, the cell shapes were quite different between the fresh nerve and the acellular nerve. Many cells in the fresh nerve showed spindle-shaped nuclei and cytoplasms, whereas round shapes were seen in the acellular nerve (Fig. 3A and 3B). Immunostaining for CD68 showed that most cells in the

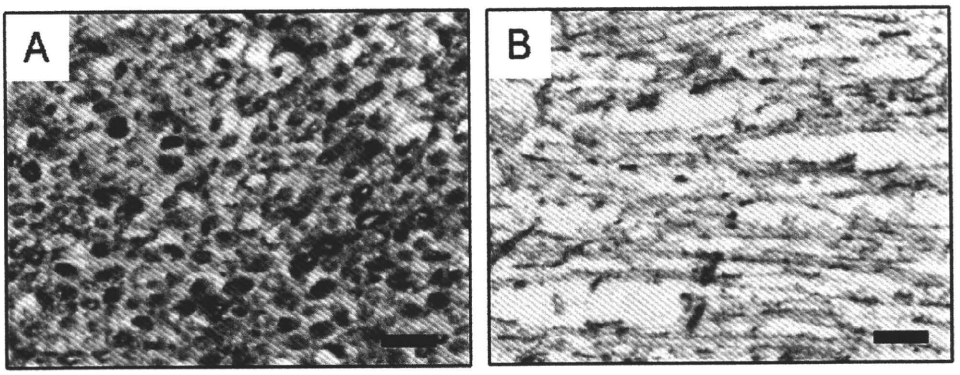

Figure 2. Immunostaining for GFAP of fresh (A) and acellular (B) nerves before implantation. Scale bars = 50 μm.

acellular nerves were macrophages while there were very few CD68-positive cells in the fresh nerves (Fig. 3C and 3D). The total numbers of cells and CD68-positive cells are summarized in Fig. 4. The total cell densities in the fresh and acellular nerves were the same. However, most cells in the acellular nerves were CD68-positive cells, whereas there were almost no CD68-positive cells in the fresh nerves. The major cell population in the fresh nerves could not be identified from immunostaining.

Angiogenesis in the graft was visualized by vWF immunostaining (Fig. 3E and 3F). When the fresh nerve was implanted, many small capillaries were present inside the graft (495 capillaries), and the surrounding subcutaneous tissue had normal vessels. On the other hand, when the acellular nerve was implanted, angiogenesis did not occur in the graft (19 capillaries), but blood vessels with a larger diameter did appear in the surrounding tissues. These observations suggest that the decellularization process might have changed the characteristics of the nerves and caused a different host body reaction in comparison to that elicited by the fresh nerves.

3.3. Histological Evaluation of the Acellular Nerve Grafts

Histological evaluation of the transplanted grafts was carried out by HE staining and immunostaining for GFAP on 110 days and 158 days after the operation (Fig. 5). Both in the fresh autograft and in the acellular allogeneic graft, remarkable cellular infiltration was observed by HE staining, even at 110 days after transplantation. Most of these cells were aligned in the longitudinal direction of the nerves, but rarely formed a fiber-like morphology at that point on time. On the other hand, 158 days after transplantation, many fibrous structures in the long-term transplantation were observed, especially in the autologous fresh nerve.

Immunostaining for GFAP in the Schwann cells in the peripheral nerves showed that the Schwann cells had infiltrated the host nerves. At 110 days post-operation,

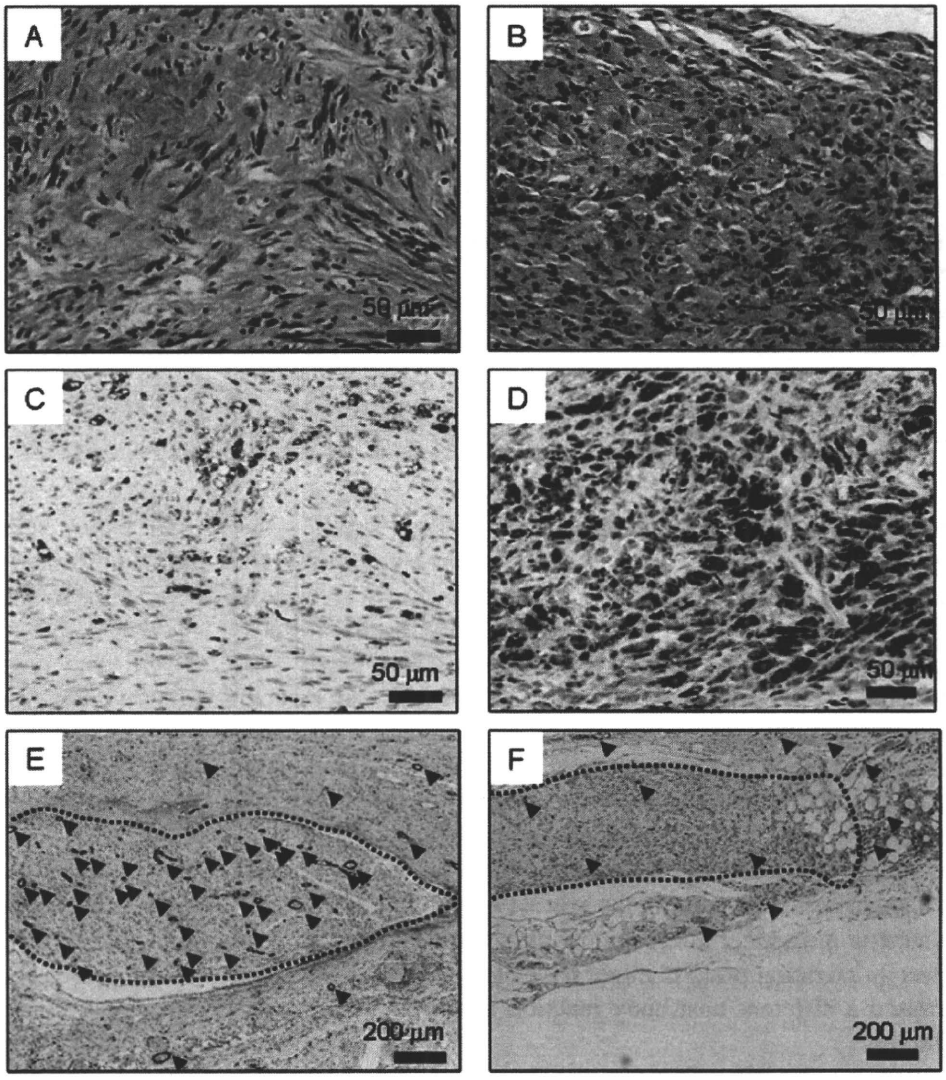

Figure 3. HE staining (A, B) and immunostaining for CD68 (C, D) and vWF (E, F) in subcutaneously implanted allogeneic fresh (A, C, E) and allogeneic acellular (B, D, F) nerves 1 month postimplantation. The images of HE staining and immunostaining for CD68 show the middle areas of the implant. The dotted lines and arrowheads in E and F indicate the edge of the grafts and microvessels, respectively. This figure is published in colour in the online edition of this journal, that can be accessed *via* http://www.brill.nl/jbs

a few GFAP-positive cells with fiber-like morphologies were observed in autologous fresh nerves but not in the allogeneic acellular graft. At 158 days after the time of transplantation, both grafts showed a fiber-like formation of GFAP-positive cells. At that time point, the acellular grafts included cells with thinner fiber-like morphology than the fresh nerves.

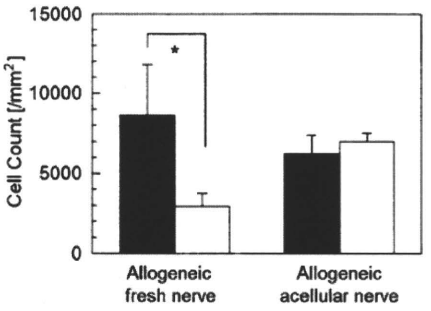

Figure 4. Number of total infiltrated cells (black column) and macrophages (white column) in the allogeneic fresh and allogeneic acellular nerves at 1-month postoperation ($n = 3$ each). Three magnified pictures were taken in each graft and the cells were counted. All data are indicated as the mean ± SD. *CD68-positive cells *vs* total cells in the fresh nerve $P > 0.05$.

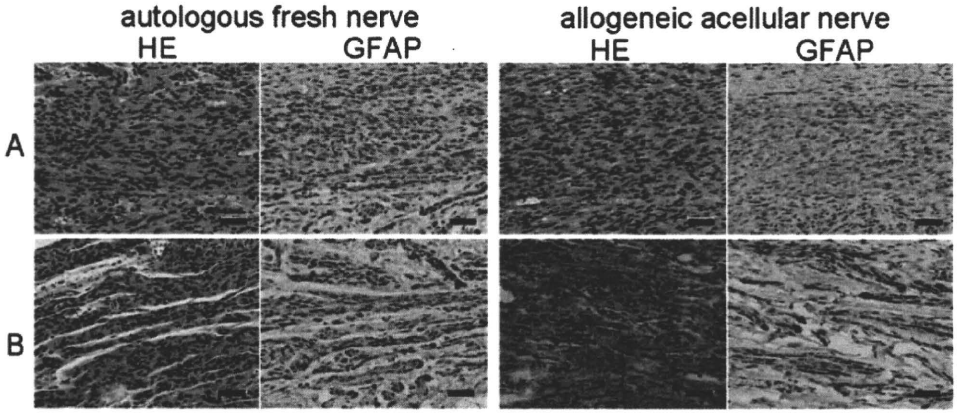

Figure 5. HE staining and immunostaining for GFAP of transplanted autologous fresh nerve and allogeneic acellular nerve (A) 110 days and (B) 158 days after operation. Scale bars = 50 μm. This figure is published in colour in the online edition of this journal, that can be accessed *via* http://www.brill.nl/jbs

3.4. Electrophysiology

Electrophysiological recovery of the allogeneic acellular nerves and autologous fresh nerves was assessed by measuring the myogenic potential of the tibial muscle group. The results from all animals subjected to the electrophysiological study are shown in Fig. 6. In the case of the autologous fresh nerves, an electrophysiological response at the tibial muscles was observed after short-term transplantation, but no reaction was seen in the acellular nerve grafts. After long-term transplantation, the electrophysiological responses in the allogeneic acellular nerve group were dramatically recovered; that is, 2 of the 3 cases showed normal reactions to the sciatic nerve stimulus (Fig. 6C). In the autologous fresh nerve group as well, only 2 of the 3 cases reacted normally to electrical stimulation. These results demonstrate that a 10-mm gap in the rat sciatic nerves can be bridged using CIP-treated allo-

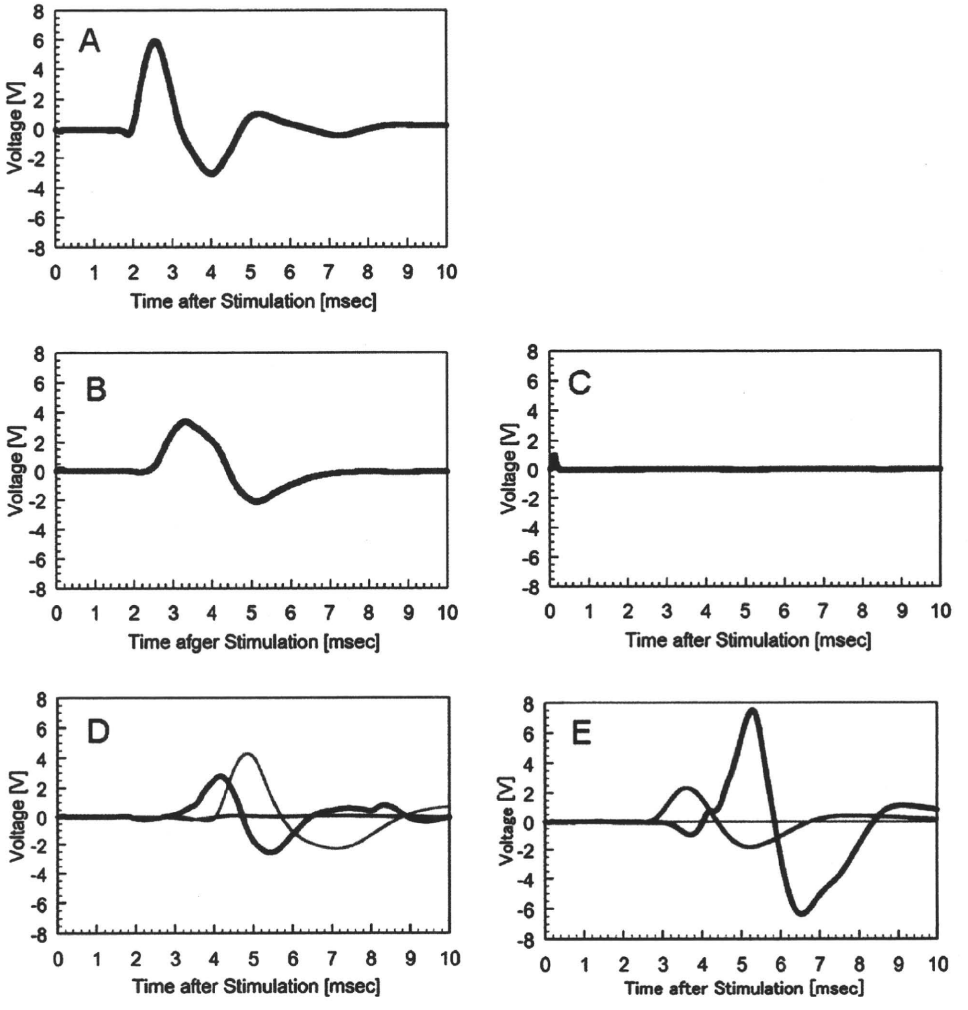

Figure 6. Averaged electromyograms of the tibial muscle of legs into which autologous fresh nerves (B, D) and allogeneic acellular nerves (C, E) were transplanted. Electromyograms before operation (A), after short-term transplantation (B, C; $n = 1$) and after long-term transplantation (D, E; $n = 3$).

geneic acellular nerves. The induced axon in that graft successfully recovered the nerve function, although the axonal growth took more time than the autologous fresh nerve did. Our results show that the myogenic potential that had completely disappeared immediately after graft transplantation was recovered thereafter.

4. Discussion

To overcome the donor shortage for peripheral nerve treatments, allogeneic acellular nerves will likely be the most viable graft for growing axons. However,

there have been only a few studies that used allogeneic animal models. In some cases, inadequate transplantation models in dogs or rats were defined as allogeneic systems [31, 33]. Rats are thought to be the best animals for investigating allogeneic transplantation because of their well-defined histocompatibility and disparity.

CIP treatment can only disrupt the cells. From this point of view, the thermal pretreatment of nerves, which is commonly used to reduce their immunogenicity, can provide the same results as our CIP treatment. However, by combining the CIP treatment with a washing process, all cells were effectively removed from the tissue. The chemical process which is commonly employed to decellularize tissue involves detergent, and that affects axonal growth. However, our washing solution did not have any such harmful component.

Electrophysiological recovery in the acellular grafts was not demonstrated in the short-term (about 5 months post-operation). It is believed that this delay of physiological recovery was caused by immature Schwann cell alignments. Although the Schwann cell alignments were observed in the acellular nerve graft 5 months after the transplantation just as in the autograft, the cells in the acellular nerve were smaller and less mature than those in the autograft. In general, from the first day to the first week following the peripheral nerve injury, macrophages are recruited in significant numbers to degenerate the axons and to remove the myelin debris for nerve regeneration. After that, the Schwann cells usually align to form pathways for the growth of axons from the proximal to distal stump of the nerve defect [34]. Thus, we evaluated the host reaction to the transplanted acellular nerves 4 weeks after implantation, since the normal reaction to injured host nerves is considered to be complete at this time point. Four weeks after the subcutaneous implantation of fresh nerves, many host cells but very few macrophages were observed in the fresh nerves (Fig. 3A and 3C), suggesting that all allogeneic cells in the transplanted nerves were removed within 1 month and replaced with the host cells. In contrast, the acellular nerves were filled with macrophages even though they did not contain any allogeneic cells when transplanted. This macrophage infiltration did not result from the incomplete removal of allogeneic cells but might have resulted from the alteration of extracellular matrix protein by CIP treatment. In fact, when the fresh and acellular nerves of SD rats were implanted in SD rats subcutaneously (isogenic transplantation), the same host reactions as in the case of the allogeneic model occurred (data not shown). It has been reported that treatment of bacteriochlorophyll with a high pressure of 0.6 GPa changed the 800-nm absorbance, reflecting a tertiary structure alteration of the protein [35]. Thus, the 980 MPa pressure used in our CIP treatment might affect the extracellular matrix structure of both allogeneic and isogenic nerves, causing them to have a much stronger foreign body reaction than that in the fresh nerve implantation. Such a large effect of CIP treatment on the ECM protein was not observed in the case of decellularization of blood vessels or cardiac valves. ECM of nerve tissue is considered to be less stable against high pressure than the fibrillar ECM of blood vessels due to the large amount of

proteoglycans. Therefore, although the acellular vessels or cardiac valves prepared by CIP treatment succeeded in tissue regeneration in animal experiments, further optimization of the CIP conditions will be needed for the nerve regeneration.

Angiogenesis is one of the inflammatory responses in material implantation. In the subcutaneous implantation study, only a low level of angiogenesis was observed in the allogeneic acellular nerves, even though many macrophages were present (Fig. 3D and 3F). On the other hand, many small vessels were observed in the allogeneic fresh nerves (Fig. 3E). We considered that the allogeneic cells were removed and host fibroblasts migrated to form granulation tissue, and then the new blood vessels were induced to provide nutritional support for these cells. In fact, different cell morphologies were observed in each of the implanted nerves (Fig. 3A and 3B). The HE staining of the allogeneic fresh nerves showed fibroblast-like cell infiltration and scar-like collagenous tissue formation in the implanted nerves, which was not observed in the acellular nerve. From these results, our acellular nerves will be suitable for nerve regeneration, even though their axonal growth was slower than that in autologous fresh nerves.

The topographical cues of nerve conduit are another important factor to be considered. A number of studies have described that the interactions between a 3-D extracellular microenvironment and axons influence neuronal growth [36]. A suitable pore size of the nerve conduits facilitates nerve regeneration. One report has shown that a macroporous synthetic nerve conduit made from poly(ε-caprolactone) with pore sizes of 1–10 μm was most effective in nerve regeneration among the bigger and smaller pore size conduits [37]. From the SEM observations, our acellular nerve had about 10 μm spaces among the remaining fibers, but failed to recover myogeneic potential even at 5 months post-operation. On the other hand, the detergent-treated allogeneic acellular nerves implanted in the 10-mm gap of a rat sciatic nerve succeeded in promoting axonal growth to the distal portion and showed good motor function, measured as electromyographic activity, within one month after the operation [20]. These good results might have arisen from the fact that their detergent-treated acellular nerves contained larger pores (20–100 μm) than our acellular nerves did. In a series of *in vitro* experiments using PC12 cells on various microchannels, Mahoney *et al.* showed that the effective widths in the neurite direction along the axis of the grooves were 20–30 μm [38]. There is expected to be a slight difference in either synthetic or tissue-derived materials between *in vivo* and *in vitro* studies. The filament diameter in the acellular nerves also affects the axonal growth activity. The optimal polypropylene filament diameter for alignment of dorsal root ganglion (DRG) neurites and outgrowth of Schwann cells has been reported to be 5 μm [39]. The combination of biomolecules with acellular nerves is expected to be another way to accelerate axonal growth. Rat acellular nerve allografts loaded with vascular endothelial growth factor and beta-nerve growth factor are reported to lead to greater axonal density at the distal portion of the graft [20].

5. Conclusion

Our allogeneic acellular nerves show promise for use as axonal scaffolds in peripheral nerve defects. As compared to allogeneic fresh nerves, the allogeneic acellular nerves did not induce scar formation in the graft, and led to a successful recovery of sciatic nerve function. Further optimization of the CIP treatment will result in fewer protein structural changes and an improvement of the spaces among the fibrous components, which may improve the regeneration rate and axon density.

Acknowledgements

This work was financially supported by a Grant-in-Aid for Young Scientists (B), a Grant-in-Aid for Scientific Research from the Ministry of Health, Labour and Welfare of Japan, and a CREST-JST grant.

References

1. J. R. Hess, M. J. Brenner, I. K. Fox, C. M. Nichols, T. M. Myckatyn, D. A. Hunter, S. R. Rickman and S. E. Mackinnon, *Plast. Reconstr. Surg.* **119**, 246 (2007).
2. D. Neubauer, J. B. Graham and D. Muir, *Exp. Neurol.* **207**, 163 (2007).
3. A. K. Gulati, *J. Neurosurg.* **68**, 117 (1988).
4. S. M. Hall, *Neuropathol. Appl. Neurobiol.* **12**, 401 (1986).
5. C. Ide, K. Tohyama, E. Yokota, T. Nitatori and S. Onodera, *Brain Res.* **288**, 61 (1983).
6. S. E. Mackinnon, V. B. Doolabh, C. B. Novak and E. P. Trulock, *Plast. Reconstr. Surg.* **107**, 1419 (2001).
7. M. Sondell, G. Lundborg and M. Kanje, *Brain Res.* **795**, 44 (1998).
8. T. W. Hudson, S. Zawko, C. Deister, S. Lundy, C. Y. Hu, K. Lee and C. E. Schmidt, *Tissue Eng.* **10**, 1641 (2004).
9. B. Hontanilla, C. Audá, J. Aucocha and O. Gorría, *Neurosurgery* **58**, 768 (2006).
10. C. B. Jenq and R. E. Coggeshall, *Brain Res.* **361**, 233 (1985).
11. T. M. Myckatyn and S. E. Mackinnon, *Neurol. Res.* **26**, 124 (2004).
12. T. Osawa, C. Ide and K. Tohyama, *Arch. Histol. Jpn* **50**, 193 (1987).
13. P. J. Evans, R. Midha and S. E. Mackinnson, *Prog. Neurobiol.* **43**, 187 (1994).
14. Z. Li, J. Peng, G. Wang, Q. Yang, H. Yu, Q. Guo, A. Wang, B. Zhao and S. Lu, *Exp. Neurol.* **214**, 47 (2008).
15. A. K. Gulati and G. P. Cole, *J. Neurosurg.* **72**, 114 (1990).
16. N. Danielsen, J. M. Kerns, B. Holmquist, Q. Zhao, G. Lundborg and M. Kanje, *Brain Res.* **681**, 105 (1995).
17. T. W. Hudson, S. Y. Liu and C. E. Schmidt, *Tissue Eng.* **10**, 1346 (2004).
18. T. Osawa, K. Tohyama and C. Ide, *J. Neurocytol.* **19**, 833 (1990).
19. J. Sørensen, K. Fugleholm, M. Moldovan, H. Schmalbruch and C. Krarup, *Brain Res.* **903**, 185 (2001).
20. B. S. Kim, J. J. Yoo and A. Atala, *J. Biomed. Mater. Res. A* **68**, 201 (2004).
21. J. M. Rovak, D. K. Bishop, L. K. Boxer, S. C. Wood, A. K. Mungara and P. S. Cederna, *J. Reconstr. Microsurg.* **21**, 207 (2005).
22. H. C. Ott, T. S. Matthiesen, S. K. Goh, L. D. Black, S. M. Kren, T. I. Netoff and D. A. Taylor, *Nature Med.* **14**, 213 (2008).

23. S. R. Meyer, J. Nagendran, L. S. Desai, G. R. Rayat, T. A. Churchill, C. C. Anderson, R. V. Rajotte, J. R. Lakey and D. B. Ross, *J. Thorac. Cardiovasc. Surg.* **130**, 469 (2005).
24. S. Mirsadraee, H. E. Wilcox, K. G. Watterson, J. N. Kearney, J. Hunt, J. Fisher and E. Ingham, *J. Surg. Res.* **143**, 407 (2007).
25. C. Ide, T. Osawa and K. Tohyama, *Prog. Neurobiol.* **34**, 1 (1990).
26. S. E. Mackinnon, A. R. Hudson, R. E. Falk, D. Kline and D. Hunter, *Neurosurgery* **15**, 690 (1984).
27. E. L. Whitlock, S. H. Tuffaha, J. P. Luciano, Y. Yan, D. A. Hunter, C. K. Magill, A. M. Moore, A. Y. Tong, S. E. Mackinnon and G. H. Borschel, *Muscle Nerve* **39**, 787 (2009).
28. T. Fujisato, K. Minatoya, S. Yamazaki, Y. Meng, K. Niwaya, A. Kishida, T. Nakatani and S. Kitamura, in: *Cardiovascular Regeneration Therapies Using Tissue Engineering Approaches*, H. Mori and H. Matsuda (Eds), p. 83. Springer, Tokyo (2005).
29. S. Hall, *J. Anat.* **190**, 57 (1997).
30. G. Keilhoff, F. Prätsch, G. Wolf and H. Fansa, *Tissue Eng.* **11**, 1004 (2005).
31. C. Ide, K. Tohyama, K. Tajima, K. Endoh, K. Sano, M. Tamura, A. Mizoguchi, M. Kitada, T. Morihara and M. Shirasu, *Exp. Neurol.* **154**, 99 (1998).
32. P. J. Evans, S. E. Mackinnon, R. Midha, J. A. Wade, D. A. Hunter, Y. Nakao and G. M. T. Hare, *Microsurgery* **19**, 115 (1999).
33. M. Nakamura, N. Tomizawa, K. Tohyama and S. Hara, *J. Vet. Med. Sci.* **66**, 767 (2004).
34. V. H. Perry, M. C. Brown and S. Gordon, *J. Exp. Med.* **165**, 1218 (1987).
35. A. Gall, A. Ellervee, J. N. Sturgis, N. J. Fraser, R. J. Cogdell, A. Freiberg and B. Robert, *Biochemistry* **42**, 13019 (2003).
36. G. N. Li and D. Hoffman-Kim, *Tissue Eng.* **14**, 33 (2008).
37. C. L. A. M. Vleggeert-Lankanp, G. C. W. de Ruiter, J. F. C. Wolfs, A. P. Pêgo, R. J. van den Berg, H. K. P. Feirabend, M. J. A. Malessy and E. A. J. F. Lakke, *J. Biomed. Mater. Res. A* **80**, 965 (2007).
38. M. J. Mahoney, R. R. Chen, J. Tan and W. M. Saltzman, *Biomaterials* **26**, 771 (2005).
39. X. Wen and P. A. Tresco, *J. Biomed. Mater. Res. A* **76**, 626 (2006).

Full Paper

Received: 11 August 2009, Revised: 1 April 2010, Accepted: 8 April 2010, Published online in Wiley Online Library: 27 May 2010

(wileyonlinelibrary.com) DOI:10.1002/cmmi.389

Design and characterization of a polymeric MRI contrast agent based on PVA for *in vivo* living-cell tracking

Yoichi Tachibana[a], Jun-ichiro Enmi[b], Atsushi Mahara[a], Hidehiro Iida[b] and Tetsuji Yamaoka[a]*

A novel water-soluble MRI contrast agent for *in vivo* living cell tracking was developed. Unlike the conventional *in vivo* cell tracking system based on superparamagnetic iron oxide beads, the newly developed contrast agent is eliminated from the body when the contrast agent exits the cells upon cell death, which makes living cell tracking possible. The contrast agent is composed of gadolinium chelates (Gd–DOTA) and a water-soluble carrier, poly(vinyl alcohol) (PVA), which is known to interact with cells and tissues very weakly. Since the Gd–PVA was not taken up by cells spontaneously, the electroporation method was used for cell labeling. The delivered Gd–PVA was localized only in the cytosolic compartment of growing cells with low cytotoxicity and did not leak out of the living cells for long periods of time. This stability may be due to the weak cell-membrane affinity of Gd–PVA, and did not affect cell proliferation at all. After cell labeling, signal enhancement of cells was observed *in vitro* and *in vivo*. These results indicate that Gd–PVA can visualize only the living cells *in vivo* for a long period of time, even in areas deep within large animal bodies. Copyright © 2010 John Wiley & Sons, Ltd.

Keywords: MRI; cell tracking; intracellular delivery; cell transplantation; Gd chelate

1. INTRODUCTION

Over the past decade, there has been increasing interest in developing cell transplantation therapy (1–3) for various diseases such as ischemic limbs (4), infarcted myocardium (5,6) and diabetic retinopathy (7). In particular, the transplantation of autologous cells such as bone marrow- or fat tissue-derived mesenchymal stem cells is much safer than heterologous transplantation in terms of rejection, and is promising in clinical use. However, the mechanism of cell transplantation therapy remains a matter of debate. One possible mechanism is the differentiation of transplanted cells into functional cells, and another is the paracrine effect due to the produced cytokines (8). Moreover, even the engraftment ratio and survival period of the transplanted cells remain unclear. A general method of analyzing the transplanted cells, such as immunostaining, cannot be used for autologous cell transplantation because there is no phenotypic difference between transplanted cells and host cells. In recent years, then, noninvasive tracking systems for cell transplantation are attracting a great deal of attention (9,10).

Optical imaging methods using fluorescence- or bioluminescence-labeled cells have been studied extensively (11,12). Recently, green fluorescent protein (GFP)-transgenic animal or GFP-positive cells have become widely available and have been easily analyzed using various *in vivo* optical imaging instruments. However, since optical lights can penetrate tissues less than 10 mm in the case of fluorescence and 30 mm in the case of bioluminescence, only mice or rats can be used in this system (13). Therefore, cell transplantation model systems cannot be used for various diseases in large animals (14–16). In addition, the resolution is low, and the transplanted cells can be detected as large circles in small animals (13).

In contrast, magnetic resonance imaging (MRI) is a more promising system because of its high resolution, its absence of limitations on animal size and its noninvasiveness. In order to detect the transplanted cells in host tissues using MRI, cells should be labeled with contrast agents. In the past 15 years, superparamagnetic iron oxide particles (SPIO) have been studied as a means of labeling cells because of their high sensitivity (17,18). SPIO are superior to other contrast agents in terms of the detection of cells. Rice *et al.* reported the homing phenomena of adipose-derived stem cells in cerebral infarction (19). Stuckey *et al.* reported the monitoring of bone marrow stromal cells in the infarcted heart (20). Targeted cells were usually labeled with SPIO by the endocytosis mechanism or by using gene-transfection agents. However, in long-term tracking of cells, one of the problems with this system is the fate of SPIO which leaks out of

* *Correspondence to: T. Yamaoka, Department of Biomedical Engineering,Advanced Medical Engineering Center, National Cardiovascular Center Research Institute, Suita 565-8565, Japan.*
E-mail: yamtet@ri.ncvc.go.jp

a *Y. Tachibana, A. Mahara, T. Yamaoka*
Department of Biomedical Engineering,Advanced Medical Engineering Center, National Cardiovascular Center Research Institute, Suita 565-8565, Japan

b *J.-i. Enmi, H. Iida*
Department of Investigative Radiology,Advanced Medical Engineering Center, National Cardiovascular Center Research Institute, Suita 565-8565, Japan

Contract/grant sponsor: Ministry of Health, Labour and Welfare of Japan (Health and Labour Sciences Research Grants, Research on Nanotechnical Medical).
Contract/grant sponsor: Research Grant for Cardiovascular Diseases, Ministry of Health, Labour and Welfare of Japan; contract/grant number: 18A-2.

cells (free SPIO) due to exocytosis or cell death. Additionally, SPIO that has undergone intracellular uptake is slowly digested, releasing its iron. The free SPIO remains in the body and continues to show MR contrast, creating the potential for misunderstanding (21). Amsalem *et al.* reported that the observed MRI signals after transplantation of SPIO-labeled MSCs were not attributed to transplanted cells but to cardiac macrophages which took up the released SPIO from transplanted cells (22). Li *et al.* reported that SPIO undergoing cell death was internalized by macrophages or remained in the local tissue (23).

The most important part of cell tracking is to track only the living cells. In the present study, a novel water-soluble contrast agent was designed and an effective intracellular delivery system was established. Gd–DOTA (1,4,7,10-tetraazacyclo-dodecane-*N,N',N'',N'''*- tetraacetic acid) was conjugated to a bioinert and highly water-soluble polymeric carrier, poly(vinyl alcohol) (PVA). PVA is known to circulate for a long period of time in the blood stream *in vivo* because of its very weak interaction with the blood cells, macrophages or tissues. It was reported that the amount of PVA ingested by macrophages was much less than that of bovine serum albumin (24). The conjugates would be expected to be eliminated from the tissues without being ingested by macrophages when they are outside of the dead cells. The intracellular delivery system of the conjugates was established using an electroporation system, and the cytotoxicity, intracellular stability, body distribution and MR-imaging ability of the contrast agent were studied *in vitro* and *in vivo*.

2. RESULTS

2.1. Synthesis of Gd–PVA (*4a–d*)

Conjugates **4a–d** were synthesized in three steps using PVA with a molecular weight of 74 800 (**1**) as shown in Scheme 1. The structure of conjugates **4a–d** was confirmed by ^{1}H-NMR spectroscopy and their characteristics are summarized in Table 1. At step 1, the introduction ratios of diamine ($m/n \times 100$ in Scheme 1) were 13.2, 7.5, 3.6 and 12.9%, respectively. At step 2, DOTA-NHS-ester was completely reacted with free NH_2 groups on **2** because the peak of 2.79 ppm had disappeared. These polymers were soluble in water and DMSO and insoluble in acetone, toluene and tetrahydrofuran. The Gd (III) content of the conjugates (**4a–d**) was analyzed by inductively coupled plasma atomic emission spectroscopy. To observe the cell labeling efficiency and the intracellular distribution of the conjugates, Gd–PVA labeled with fluorescence (**4d**) was synthesized. MR imaging of labeled cells was carried out after confirming the cell uptake of **4d** with fluorescent microscopy. By contrast, the cytotoxicity assay was performed using **4b** without FITC because the wavelength of FITC overlapped with that of the WST assay.

The increase of the relaxivities (R_1) of **4a–d** with the increased introduction ratio of DOTA may be due to an increased rotational correlation and constructive restriction of motion. A maximum reflexivity value of 7.1 $mM^{-1}\,s^{-1}$ was observed at 13.2 mol% (**4a**). All of the relaxivities of **4a–d** were higher than that of clinically used Gd–DTPA (5.1 $mM^{-1}\,s^{-1}$), suggesting that each conjugate can be used as an effective contrast agent.

2.2. *In vitro* T_1-weighted MR measurements of polymer solutions

Figure 1 shows the MR images of **4d** solutions with different concentrations at 4.7 T. The T_1-weighted MRI signal of the **4d** solution increased with the increased polymer unit concentration. Significant contrast enhancement was seen over 0.2 mM. To achieve cell imaging, it is necessary to introduce the contrast agents at sufficient concentrations in the cells.

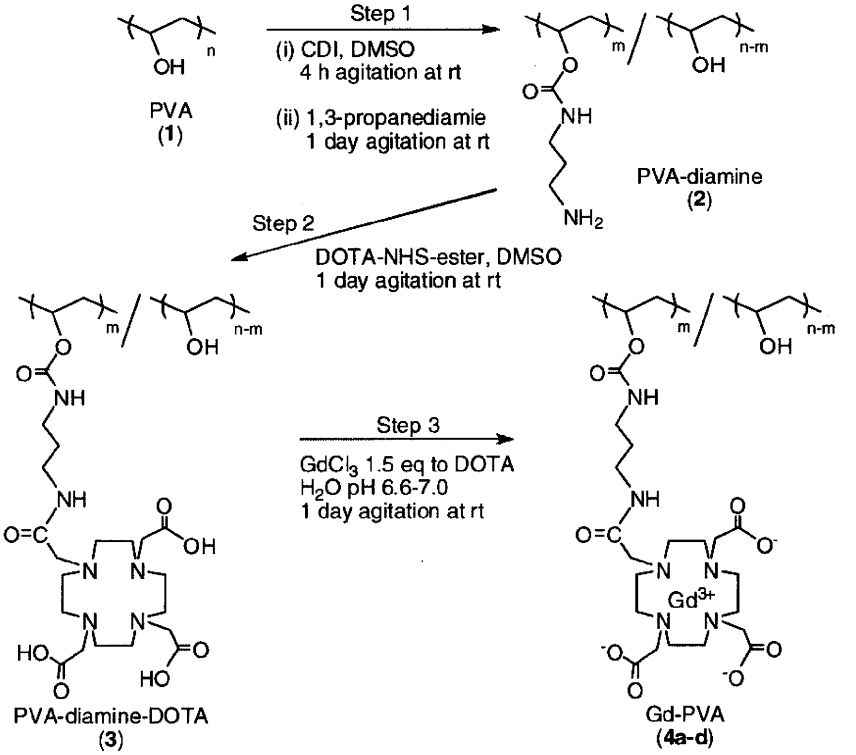

Scheme 1.

Table 1. Synthesis of **4a–d** with different contents of gadolinium chelates

	Introduction ratio of DOTA[a] (mol%)	Mn[b] ($\times 10^5$)	M_w/M_n[b]	Gd[c] (wt%)	Gd/DOTA (mol%)	FITC label	R_1 (mM^{-1} s^{-1})
4a	13.2	1.6	1.1	12.0	70.0	–	7.1
4b	7.5	1.1	1.2	9.2	69.1	–	6.2
4c	3.6	1.2	1.2	5.8	67.0	–	6.2
4d	12.9	—	—	9.3	53.9	+	7.0

[a]Scheme 1, $m/n \times 100$.
[b]Determined by size exclusion chromatography using 0.25 mM phosphate buffer as eluent with polystyrene standards.
[c]Determined by inductively coupled plasma atomic emission spectroscopy measurement.

2.3. Cytotoxicity of Gd–PVA to NIH-3T3 cells and cell labeling by electroporation

Gd–PVA **4b** was used for a cytotoxicity assay since FITC introduced to **4d** obstructs the accurate WST-1 assay. The viability of NIH-3T3 cells in the presence of **4b** was not affected even at high concentrations (10 mM; polymer unit concentration in culture medium) for up to 3 days (see Supplementary Information). The low affinity of PVA (24) might suppress the interaction of Gd–PVA with the cell membrane and decrease the cytotoxicity. In fact, weak interaction was demonstrated by a simple experiment as follows. Compound **4d** was added to the culture medium of NIH-3T3 cells, and the cells were incubated for 1 h. After washing with PBS three times, no fluorescence induced by **4d** was observed, indicating that **4d** was unable to attach to the cell membrane or enter the cells spontaneously.

To deliver such a bio-inert substance into cells, we selected an electroporation method that is mainly used to transfect DNA into cells. Since this method can introduce a large amount of polymeric substances into any kind of cells nonspecifically with low cytotoxicity, it is suitable for labeling various cells including established cell lines, somatic stem cells, or even embryonic stem cells for cell transplantation (25,26). When electroporation was carried out, the concentration of Gd–PVA in culture medium was set to 10 mM (polymer unit concentration) based on the result of the cytotoxicity assay.

Figure 2 shows bright field and fluorescent photomicrographs of NIH-3T3 cells 3 days after electroporation with **4d**. Almost all cells were labeled efficiently, and the intracellular **4d** was interestingly located only in the cytosolic compartment of NIH-3T3 cells even after cell proliferation. This intracellular distribution pattern is different from that for endocytosis, which is made from bright dots.

The stability of Gd–PVA in NIH-3T3 cells was assessed by measuring the total fluorescence intensity of the growing NIH-3T3 cells with time. The number of Gd(III) molecules in one cell calculated from the fluorescence intensity was 7.3×10^8 per cell just after electroporation. Cells were cultured for a given period of time without subculture and then lysed. Before the cells were lysed, they were washed by PBS sufficiently to eliminate any **4d** leaching from them. Figure 3 represents the total fluorescence intensity of **4d** in NIH-3T3 cells (solid circle) and cellular proliferation rates (open circle). Fluorescence derived from **4d** in cells showed no significant change over 10 days, and the labeled cells grew well. These results show that **4d** can remain in the cytosolic compartment stably for a long period of time without having any effect on cell proliferation.

2.4. *In vitro* T_1-weighted MR measurements of the labeled NIH-3T3

Figure 4a shows an MR image of the NIH-3T3 cell suspensions at 4.7 T. Compound **4d**-labeled NIH-3T3 cell suspension, non-labeled NIH-3T3 cell suspension and cell-free and Gd-free medium were left at rest for 1 day to allow the cells to be precipitated to the bottom of the test tube. Clear signal enhancement in tube 1 at slice B passing through the precipitated cells was seen. On the other hand, no signal was observed in tube 1 at slice A, which indicates that **4d** did not leak out of the cells and that **4d** in cells gives sufficient MR contrast irrespective of the small amount of free water in the cells

To examine the cell density dependence of signal enhancement, we next acquired MR images of **4d**-labeled NIH-3T3 cells at different densities in agarose gel, which was used to fix the transplanted cells in the experiment involving the injection of cells into a rat (Fig. 4b). MRI can depict at least 3.5×10^6 NIH-3T3

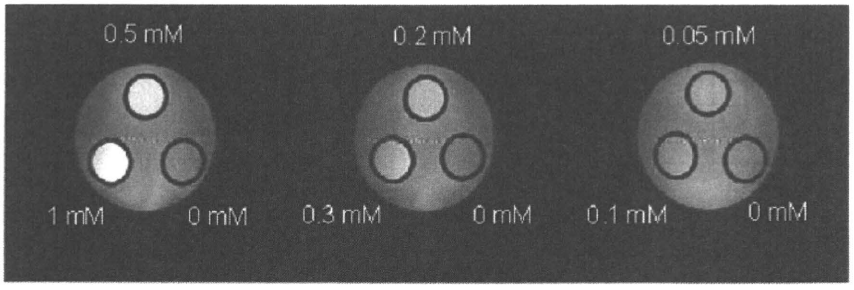

Figure 1. *In vitro* T_1-weighted MR measurements of **4d** in water at 4.7 T at the concentrations of 0, 0,05, 0.1, 0.2, 0.3, 0.5, and 1.0 mM. Three test tubes containing different concentrations were fixed vertically. A horizontal section was scanned. These images were acquired using a 2 D spin echo sequence with a TR of 2000 ms and a TE of 16 ms. These images were displayed using the same window level and window width.

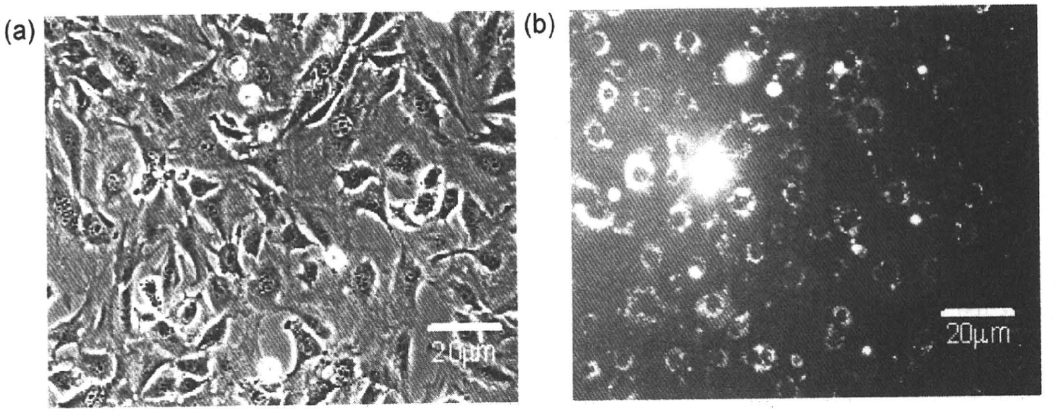

Figure 2. (a) Phase image and (b) fluorescent image of NIH-3T3 cells labeled with **4d** (FITC-Gd-PVA) at 3 days after electroporation. After electroporation, cells were washed three times by PBS. The bright ring forms showed cytosolic compartments in the fluorescent image. The scale bar represents 20 μm.

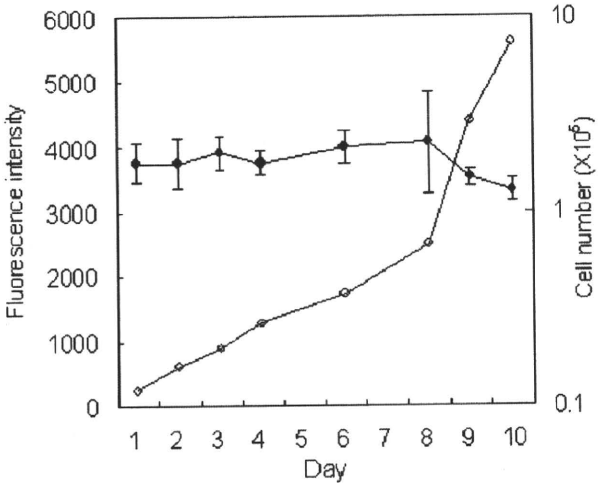

Figure 3. Changes in fluorescence intensity of **4d** existing in total NIH-3T3 cells in culture (solid circle) and the number of cells (open circle) measured over the course of the 10 days following electroporation. Fluorescence intensity is proportional to the amount of **4d** in total cells.

cells. The number of cells transplanted to the rat ischemic hind limb model (27) or infarcted myocardium swine model (28) was 1×10^7 or 5×10^7, respectively. The sensitivity shown in Fig. 4 revealed that our imaging agent would surely be useful for tracking this range of transplanted cells *in vivo*. Future studies should focus on high labeling efficiency at higher concentrations of **4d** using electroporation or another method.

2.5. *In vivo* fate of free SPIO and free Gd–PVA

To detect the living cells, contrast agents present outside of the labeled cells (free contrast agent) after cell death should be eliminated from the transplantation site. Solutions of **4d** and SPIO injected into the tissue were used as the model for free contrast agents. Solutions of **4d** and SPIO were directly injected into rat femoral muscles, and on days 0, 3 and 6, the MR image was analyzed (Fig. 5). Representative slices are shown in Fig. 5. The bright signal attributed to **4d** weakened rapidly and was observed only slightly on day 3. In contrast, the dark signal due to SPIO remained in the same area and was clearly observed even 10 days after the injection. The same tendency was observed in the other slices. SPIO-derived contrast several days after injection may be attributed to the phagocytes engulfing the injected SPIO, as has been previously reported (22,23). Furthermore, the time courses of the contrast-to-noise ratio (CNR) and the volume of the contrast-enhanced region were evaluated (Fig. 6). For SPIO, the CNR and the volume of the contrast-enhanced region showed no significant decrease over the course of 13 days. In contrast, these same parameters decreased rapidly when **4d** was used. Signal enhancement was observed in only one out of three rats at 4 days after injection. Therefore, the data of **4d** at 4 days have no error bar. Signal

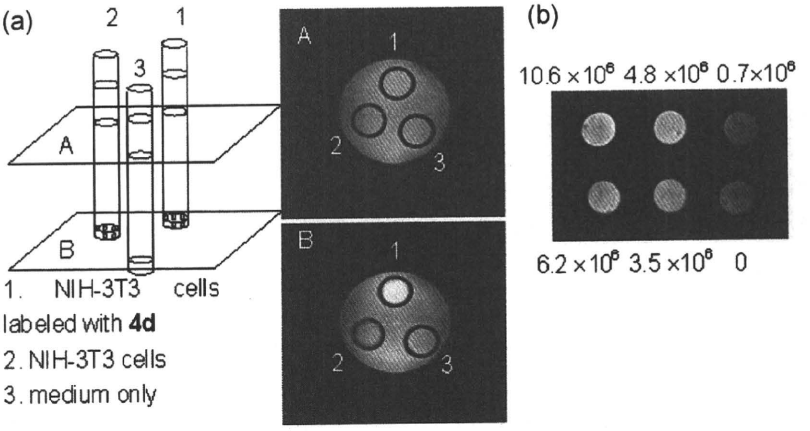

Figure 4. (a) *In vitro* T_1-weighted MR measurements of **4d**-labeled NIH-3T3 cells (tube 1), unlabeled NIH-3T3 (tube 2), and medium (tube 3) at 4.7 T. (b) *In vitro* T_1-weighted image of different numbers of cells labeled with **4d** suspended in 100 μl agarose gel.

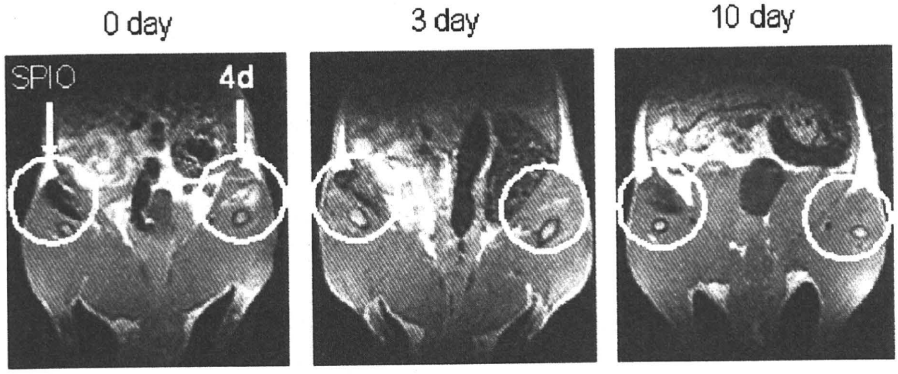

Figure 5. *In vivo* MR measurements after the injection of **4d** solution and SPIO solution into rat femoral muscle at 1.5 T. These images showed the slices passing though the injection site. These images were obtained with a TR of 1500 ms and a TE of 9 ms (FOV, 4 × 8 cm; matrix, 128 × 256; slice thickness, 1 mm; slice gap, 0 mm; number of slices, 35).

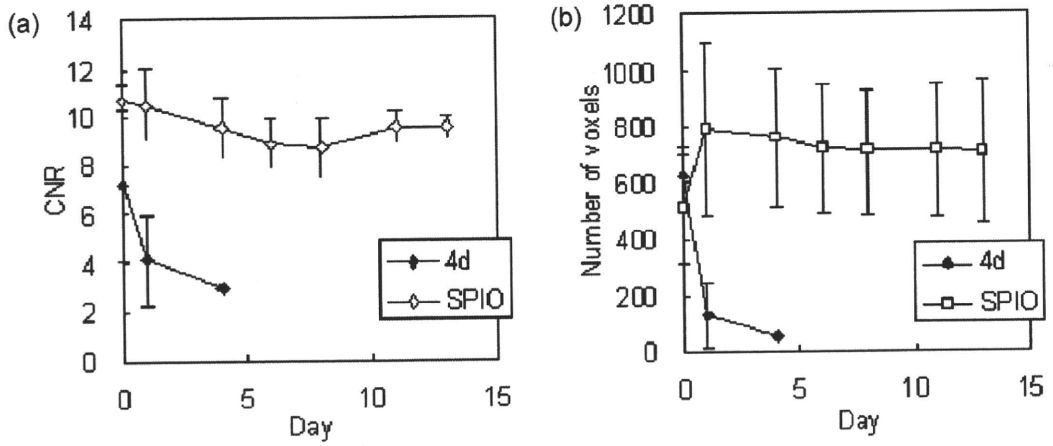

Figure 6. The time course of (a) the contrast-to-noise ratio (CNR) and (b) the number of voxels in the region where bright or dark signals due to contrast agents were observed. Contrast enhancement due to **4d** and SPIO was assessed using T_1- (TE 9 ms, TR 500 ms) and T_2- (TE 20 ms, TR 3 s) weighted images, respectively. The other scanning parameters were the same as in Figure 5. Three rats were examined and treated in the same manner as in Figure 5. CNR was calculated as $(\pi/2)^{1/2}|S_1\text{-}S_2|/S_{air}$, where S_1, S_2 and S_{air} were the mean intensities in the contrast-enhanced region, muscle and air, respectively.

enhancement due to **4d** disappeared completely in all rats at 6 days after injection. These data showed the rapid clearance of Gd–PVA from muscle and the long-term retention of SPIO in muscle. Yamaoka *et al.* reported that the half-life period of radio-labeled PVA (molecular weight of 74 800) after i.m. injection was about 10 h (38). As shown in Fig. 6, the half-life period of free Gd–PVA from the tissue was about 10 hs, which was almost the same as that of PVA. This result suggested that free Gd–PVA behaved like free PVA without interacting with macrophages *in vivo*. It can then be considered that the MR contrast of Gd–PVA is attributable to the living cells *in vivo*.

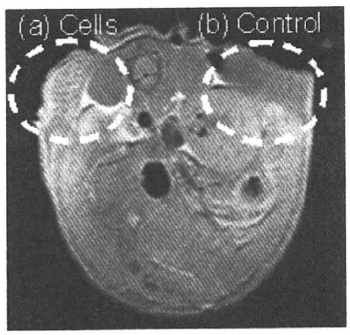

Figure 7. Preliminary *in vivo* T_1-weighted MR measurements of **4d**-labeled NIH-3T3 cells implanted in mice subcutaneously at 2 T. These cells were fixed in agarose gel. (a) 2×10^7 of **4d**-labeled cells suspended in 200 μl agarose gel (b) 200 μl agarose gel only. T_1-weighted images were acquired using a 2D spin echo sequence with a TR of 2000 ms and a TE of 9 ms (FOV, 3 × 6 cm; matrix, 128 × 256; slice thickness, 1 mm) at room temperature.

2.6. Preliminary *in vivo* MR imaging of transplanted NIH-3T3 cells

Figure 7 shows an MR image of a rat that received subcutaneous transplantation of 2×10^7 **4d**-labeled NIH-3T3 cells entrapped in agarose gel and cell-free gel (control) at each side of the back. In this preliminary MR imaging, we used undegradable agarose gel to evaluate the MRI contrast at a known density of cells. Strong contrast enhancement was observed at the area where labeled NIH-3T3 cells were transplanted, while the control gel revealed a dark shadow. These results indicate that transplanted cells can be detected *in vivo* at a cell density of 10^7 cells per 0.1 ml.

3. DISCUSSION

Our goal was to track only the living cells *in vivo* for a long period of time. To this end, an MRI contrast agent with adequate

characteristics for cell labeling and delivery system into the cells is a key factor. Cell labeling using SPIO as a contrast agent was reported in detail by Engberink *et al.* in 2007 (29). They cocultured human monocytes with SPIO suspension at a concentration of 1.0 mg Fe ml^{-1} for 0–6 h. Incubation with SPIO resulted in effective cell labeling by endocytosis, nonspecifically. The detection limit was 0.5×10^6 labeled cells per 250 μl on a 4.7 T MRI scanner. SPIO permits the detection of a small number of cells because of its high sensitivity. In general, however, endocytosed substrates would be exocytosed over time. The MR contrast obtained after SPIO-labeled cell transplantation was not attributed to the transplanted cells but to the macrophages that engulfed the free SPIO (22,23). In this study, MR imaging data for SPIO solution in femoral muscle showed that, even at 10 days after injection, SPIO still remained. These data suggested that SPIO is less suitable for long-term cell tracking. To track the transplanted cells for a long period of time, the labeling agent released upon cell death should be eliminated from the tissue.

Since we found that low-molecular-weight Gd-chelates cannot remain in cells stably (data not shown), water-soluble conjugates of Gd-chelates and a bio inert water-soluble carrier were designed. The characteristics of Gd-containing conjugates including the body distribution pattern are affected by the nature of the carrier polymer. The water-soluble contrast agent is expected to be eliminated from the body once it exits the cells if a truly bio-inert carrier molecule is selected. To track only the living cells, the contrast agents should be designed to be different from the conventional water-soluble imaging agent for vascular inflammation imaging or vascular imaging (30–36).

We selected PVA in this experiment as the carrier material for long-term living cell tracking. Selecting nondegradable PVA as the carrier enabled us to evaluate the potential of the contrast agent in intracellular distribution or in cell tracking for a long period of time. The body distribution of various polymeric carriers has been extensively studied (37,38). Among these carriers, PVA has various advantages as a candidate for use in the biomedical and pharmaceutical fields. Some of these advantages include its characteristics of water solubility, nontoxicity and noncarcinogenicity. The half-life of Gd–PVA was longer than those of other polymers such as dextran, pullulan and gelatin because of an insignificant interaction with macrophages and blood cells (24). This weak interaction with various cells is believed to be responsible for the high hydrophilicity of PVA. Since we proposed novel contrast agents in the present study that would not exit the cells for long-term cell tracking, this weak interaction with the cell membrane was considered to be an advantage.

In the present study, we chose electroporation as a method for delivering Gd–PVA into cells in order to establish a method that is applicable to a variety of cells such as stem cells and primary cells. The material delivery efficiency into cells via nonspecific endocytosis or receptor-mediated encodytosis is probably affected by the cell type. Interestingly, Gd–PVA delivered into cells was localized only in the cytosolic compartment even after cell proliferation (Fig. 2), although the reason for this remains unclear.

One possible issue in living cell tracking, although unlikely to occur, is the uptake of dying cells labeled with **4d** by tissue macrophages that remain in the tissue. To study this possibility, it is necessary to perform an experiment using cells in different states (viable, dying and dead). However, it is difficult to control the states of transplanted cells. We are considering evaluating the effect of macrophages on the fate of Gd–PVA by transplanting irradiated cells with sublethal doses or by xenografting Gd–PVA-labeled cells.

Long-term cell tracking will be feasible due to the high stability of Gd–PVA in cells for a long period of time (Fig. 3). In contrast to SPIO, the free Gd–PVA will be eliminated from the tissue (Fig. 5) when the transplanted cells burst upon cell death. The imaging of only the living cells might be achieved using Gd–PVA.

4. CONCLUSION

The novel MRI contrast agents composed of PVA and Gd showed high relaxivity and low cytotoxicity. The growing rate of NIH-3T3 cells was not affected by the intracellularly delivered Gd–PVA. Furthermore, Gd–PVA was retained stably in cells for at least 10 days. The *in vitro* T_1-weighted MR measurements using NIH-3T3 cells revealed that cells could be visualized under MRI. This *in vivo* study demonstrates for the first time that Gd–PVA has high applicability as a novel contrast agent for tracking only living cells.

5. MATERIALS AND METHODS

5.1. Materials

PVA (M_w: 74,800, degree of saponification 98%) was a kind gift from Kuraray Co. Ltd (Okayama, Japan). 1,4,7,10-Tetraazacyclododecane-1,4,7,10-tetraacetic acid mono(*N*-hydroxysuccinimidyl ester) (DOTA-NHS-ester) was purchased from Macrocyclics (Dallas, TX, USA). FITC-NHS-ester was purchased from Invitrogen (Eugene, OR, USA). Gadolinium chloride ($GdCl_3$) was purchased from Wako Pure Chemical Industries (Osaka, Japan). Resovist was purchased from Nihon Schering (Osaka, Japan). Other reagents and solvents were commercially available and used as received.

5.2. Synthesis of Gd–PVA

The synthetic route and structure of polymeric contrast agents with different introduction ratios of Gd are shown in Scheme 1. A mixture of PVA (**1**; 0.44 g, 10 mmol in monomer unit concentration) and carbonyl diimidazole (5, 7.5, and 10 mmol) was stirred in 80 ml of anhydrous dimethylsulfoxide (DMSO) at room temperature under a nitrogen atmosphere for 4 h. Then, 1,3-propanediamine (50, 75, and 100 mmol) was added to the mixture, further stirred at room temperature for 1 day, and dialyzed with Spectra/Pore membrane (cut-off molecular weight = 1×10^4; Spectrum Laboratories Inc., Rancho Dominguez, CA, USA) in distilled water three times. The remaining solution was lyophilized to give **2**.

^{1}H NMR (D_2O): $\delta = 4.92$ (br, CH_2CHO), 3.92 (br, CH_2CHOH), 3.10 [br, $C(=O)NHCH_2$], 2.79 (br, CH_2NH_2), 1.57 (br, $CHCH_2$, br, $CH_2CH_2CH_2$). The introduction ratios were calculated as the ratio of the integrals of the peaks at 2.79 and 1.57 ppm.

PVA-diamine was reacted with DOTA-NHS-ester (NH_2 of FITC-PVA-diamine: DOTA-NHS-ester = 1:1.5) in 80 ml of anhydrous DMSO at room temperature for 1 day under a nitrogen atmosphere. The reaction mixture was dialyzed in distilled water three times, and lyophilized to give PVA-diamine-DOTA (**3**).

^{1}H NMR (D_2O): $\delta = 5.07$ (br, CH_2CHO), 4.06 (br, CH_2CHOH), 3.86 [br, $C(=O)CH_2N$)] 3.51 [br, $NCH_2C(=O)OH$], 3.24 [br, $C(=O)NHCH_2$, br, CH_2CH_2N], 1.69 (br, $CHCH_2$, br, $CH_2CH_2CH_2$).

The solution of **3** was then treated with the dropwise addition of 1.5 mole equiv. of gadolinium chloride to the DOTA while stirring. The pH was maintained between 6.6 and 7.0 with 1 M NaOH solution and stirred for an additional 24 h at room temperature. The reaction mixture was dialyzed in distilled water three times and lyophilized to give Gd–PVA (**4a–d**).

For labeling Gd–PVA with FITC, PVA–diamine was mixed with a small amount of FITC–NHS–ester (NH_2 of **2**: FITC–NHS–ester = 1: 8×10^{-5}) and stirred in 80 ml of anhydrous DMSO at room temperature for 1 day under a nitrogen atmosphere. The reaction mixture was dialyzed, lyophilized to give FITC-PVA-diamine and subjected to the DOTA reaction as shown in Scheme 1.

5.3. Measurements

^{1}H-NMR spectra were recorded on a 300 MHz NMR spectrometer (Gemini2000/300; Varian Inc., CA, USA) with a sample concentration of 8 mg per 800 μl. Size exclusion chromatography analysis was carried out using Shimadzu Gel Permeation Chromatography System apparatus equipped with a refractive index and UV detectors under the following conditions: TSKgel G6000PWXL and G3000PWXL columns and 0.067 M PBS eluent at a flow rate of 0.3 ml min^{-1} at 40°C (Tosoh, Tokyo, Japan) with a sample concentration of 1 mg per 100 μl. The concentration of the paramagnetic species [Gd(III)] was measured by inductively coupled plasma atomic emission spectroscopy (model 7510, Shimadzu Co., Kyoto, Japan).

5.4. Relaxivity of conjugated Gd at 7.1 T

Solvent longitudinal relaxation times (T_1) in the aqueous solutions of the gadolinium conjugate were measured at different concentrations of gadolinium conjugate using a mixture of distilled water (0.625%) and deuterium oxide (99.375%) as a solvent. All measurements were performed on a 300 MHz (7.1 T) NMR spectrometer (Gemini2000/300; Varian Inc., CA, USA) using an inversion recovery technique with 19 inversion times (*TI*) ranging from 1 to 5000 ms at ambient temperature (25°C) with a sample concentration of 8 mg per 800 μl. A typical pulse width of 180° pulse was 19 μs. T_1 values were estimated using least-squares fitting of the signal intensities measured at 19 *TI* values in an exponential fashion. The relaxivity of each gadolinium complex was determined by a linear regression of the $1/T_1$ vs the gadolinium complex concentration.

5.5. Cell culture

NIH-3T3 cells were used for evaluating the cytotoxicity, cell labeling potential and imaging efficiency of the Gd–PVA. They were grown in Dulbecco's modified Eagle's medium (DMEM-LG) supplemented with 10% bovine calf serum, 100 units ml^{-1} penicillin, and 100 units ml^{-1} streptomycin at 37°C, 10% CO_2 atmosphere.

5.6. Cytotoxicity assay

NIH-3T3 cells (1×10^4 cells per well) were seeded in a 96-well culture plate and cultured overnight. Varying concentrations (polymer unit concentrations of 10 nM to 10 mM) of **4b** were added to each well. At the indicated time points, the number of cells was measured by WST-1 assay according to the manufacturer's protocol (Takara Shuzo, Otsu, Japan). Briefly, cells were washed with PBS three times, and the culture medium (100 μl) was added to each well. Ten microliters of WST-1 {4-[3-(4-iodophenyl)-2-(4-nitrophenyl)-2H-5-tetrazolio]-1,3-benzene disulfonate} solution was added to each well, and the plates were incubated for 30 min. The absorbance at 450 nm was measured on a microplate reader (Model 550, Bio-Rad Laboratory Co., Tokyo, Japan).

5.7. Cell labeling by electroporation

NIH-3T3 cells were cultured in a 6 cm diameter Petri dish at a concentration of 5×10^5 cells per dish in DMEM-LG for 1 day. An arbitrary amount of **4d** was added to the culture medium, and electrical pulses were applied to cells using a CUY-21 electroporator (CUY-21; NEPPA GENE, Tokyo, Japan). Rectangular electrical pulses (field strength 300 V cm^{-1}, number of pulses 10, pulse duration 5 ms) were applied to cells using two parallel electrodes with a 5 mm gap. Cells were incubated for 1 h and washed with PBS twice.

5.8. Stability of 4d in cells

To determine whether **4d** molecules stay in NIH-3T3 cells for a long period of time, the labeled cells (1×10^4 cells) were seeded in a 6 cm diameter Petri dish and cultured over 10 days without a subculture. The time course of the fluorescence intensity for the cultured cells was measured as follows. Before each measurement, cells in one dish were washed three times with PBS to eliminate the free **4d** from the cells and lysed in 1 ml lysis buffer [25 mM tris (pH 7.8), 2 mM dithiothreitol, 2 mM 1,2-diaminocyclohexan-*N,N,N',N'*-tetraacetic acid, 10% glycerol, 1% Triton X-100]. After 1 h incubation at 37°C, the fluorescence intensity of the cell lysates was measured with a spectrofluorometer (excitation 430 nm, emission 540 nm, Wallac 1420 ARVOsx, Perkin-Elmer Life Sciences, Boston, MA, USA). The time course of the fluorescence intensity represented the stability of **4d** in the cells. At the same time, the number of cells in each dish was counted. In addition, the amount of **4d** delivered into each cell by electroporation was calculated using the standard curve of fluorescence intensity.

5.9. MR imaging of Gd–PVA solution at 4.7 T

MR images of **4d** aqueous solutions were obtained on a 200-MHz (4.7 T) NMR spectrometer (Apollo; Tecmag Inc., TX, USA) equipped with a gradient system (Jeol Ltd, Tokyo, Japan; maximum gradient strength 20 mT m^{-1}; slew late 50 mT m^{-1} ms^{-1}) using a saddle coil with an inner diameter of 47 mm. Aqueous solutions with different concentrations (0.05, 0.1, 0.2, 0.3, 0.5 and 1 mM) of polymer unit were prepared. Three test tubes with different concentrations were fixed vertically. A horizontal section was scanned. T_1-weighted images of the samples were acquired using a 2D spin echo sequence with a repetition time (*TR*) of 2000 ms and an echo time (*TE*) of 16 ms. Taking the long T_1 of the water observed in the 1.5 T machine into account, *TR* was greater in comparison to that for general T_1-weighted images. We used the minimum possible *TE* to minimize the T_2 relaxation effect. Other scanning parameters were as follows: field of view (FOV), 6 × 6 cm; matrix, 256 × 256; slice thickness, 1 cm.

5.10. MR imaging of NIH-3T3 cells *in vitro*

MR measurements of labeled cells were performed using the same scanner and the same parameters as in the imaging of **4d** solutions. Cells labeled with **4d** by electroporation were trypsinized, centrifuged and resuspended in test tubes (75 mm